Supplementary information for: Extreme quantum nonlinearity in superfluid thin-film surface waves

Y. L. Sfendla[1], C. G. Baker[1], G. I. Harris[1], L. Tian[2], R. A. Harrison[1], and W. P. Bowen[1]

Corresponding author: y.sfendla@uqconnect.edu.au

[1] *ARC Centre of Excellence for Engineered Quantum Systems, School of Mathematics and Physics, The University of Queensland, Brisbane 4072, Australia*

[2] *School of Natural Sciences, University of California, Merced, California 95343, USA*

1. Supplementary Methods

Nonlinear spring constants for a superfluid thin film

As detailed in the main text, the linear spring constant k, cubic nonlinearity β and quartic (Duffing) nonlinearity α for a superfluid surface wave of amplitude $\eta[r,\theta]$ are given by

$$k = \frac{3\,\rho\,a_{\mathrm{vdw}}}{d^4} \int_0^{2\pi} \int_0^R \frac{\eta^2[r,\theta]}{\eta^2[R,0]}\, r\,\mathrm{d}r\,\mathrm{d}\theta, \quad (1)$$

$$\beta = -\frac{6\,\rho\,a_{\mathrm{vdw}}}{d^5} \int_0^{2\pi} \int_0^R \frac{\eta^3[r,\theta]}{\eta^3[R,0]}\, r\,\mathrm{d}r\,\mathrm{d}\theta \quad (2)$$

and

$$\alpha = \frac{10\,\rho\,a_{\mathrm{vdw}}}{d^6} \int_0^{2\pi} \int_0^R \frac{\eta^4[r,\theta]}{\eta^4[R,0]}\, r\,\mathrm{d}r\,\mathrm{d}\theta. \quad (3)$$

In order to reveal the explicit dependence of the (non)linear spring constants on R, d, μ and ν, we evaluate the integrals further.

The integrals in equations (1–3) can be written jointly as a function $\Phi_{\mu,\nu}^{(p)}$ with $p = 2, 3$ and 4, with

$$\Phi_{\mu,\nu}^{(p)} := \int_0^{2\pi} \int_0^R \frac{J_\mu^p\left[\zeta_{\mu,\nu}\frac{r}{R}\right]\cos^p(\mu\theta)}{J_\mu^p[\zeta_{\mu,\nu}]}\, r\,\mathrm{d}r\,\mathrm{d}\theta. \quad (4)$$

The integral over the angular coordinate θ in Eq. (4) is

$$\int_0^{2\pi} \cos^p(\mu\theta)\,\mathrm{d}\theta$$

$$= 2\pi\left(\delta_{\mu0} + (1-\delta_{\mu0})(1-\delta_{p3})\frac{(p-1)!!}{p!!}\right) \quad (5)$$

$$= \left\{\pi(1+\delta_{\mu0}),\, 2\pi\delta_{\mu0},\, \pi\frac{3+5\delta_{\mu0}}{4}\right\} \text{ for } p = \{2,3,4\}, \quad (6)$$

where we have introduced the Kronecker delta function δ. Observe here: the reduction of this integral to $2\pi\delta_{\mu0}$ for $p=3$ implies that $\Phi_{\mu\neq0,\nu}^{(3)} = 0$, so the cubic nonlinearity β vanishes for all but the zeroth-order ($\mu=0$) superfluid modes.

We can rewrite the remainder of Eq. (4) by substitution of the integrand:

$$J_\mu^{-p}[\zeta_{\mu,\nu}] \int_0^R J_\mu^p\left[\zeta_{\mu,\nu}\frac{r}{R}\right] r\,\mathrm{d}r$$

$$= \frac{\int_0^{\zeta_{\mu,\nu}} J_\mu^p[q]\, q\,\mathrm{d}q}{\zeta_{\mu,\nu}^2 J_\mu^p[\zeta_{\mu,\nu}]}\, R^2$$

$$:= \phi_{\mu,\nu}^{(p)}\, R^2. \quad (7)$$

It follows immediately that all spring constants k, β and α scale with the square of the confinement radius:

$$\Phi_{\mu,\nu}^{(p)} = 2\pi\left(\delta_{\mu0} + (1-\delta_{\mu0})(1-\delta_{p3})\frac{(p-1)!!}{p!!}\right)\phi_{\mu,\nu}^{(p)}\, R^2. \quad (8)$$

The constants $\phi_{\mu,\nu}^{(p)} = \frac{\int_0^{\zeta_{\mu,\nu}} J_\mu^p[q]\, q\,\mathrm{d}q}{\zeta_{\mu,\nu}^2 J_\mu^p[\zeta_{\mu,\nu}]}$ are tabulated in Table 1 for the three lowest mode orders μ and ν.

It is worth noting here that for $p = 2$, i.e., for the spring constant k, a closed-form expression exists for the integral $\int_0^{\zeta_{\mu,\nu}} J_\mu^p[q]\, q\,\mathrm{d}q$. In that case, we find

$$\int_0^{\zeta_{\mu,\nu}} J_\mu^2[q]\, q\,\mathrm{d}q = \frac{\zeta_{\mu,\nu}^2}{2}\left(J_{\mu-1}^2[\zeta_{\mu,\nu}] + J_\mu^2[\zeta_{\mu,\nu}]\right)$$

$$\qquad - \mu\,\zeta_{\mu,\nu} J_{\mu-1}[\zeta_{\mu,\nu}]\, J_\mu[\zeta_{\mu,\nu}]$$

$$= \frac{\zeta_{\mu,\nu}^2 - \mu^2}{2} J_\mu^2[\zeta_{\mu,\nu}],$$

where we took advantage of the Bessel function recurrence relations and our definition $J_\mu'[\zeta_{\mu,\nu}] = 0$ so that $J_{\mu-1}[\zeta_{\mu,\nu}] = \frac{\mu}{\zeta_{\mu,\nu}}J_\mu[\zeta_{\mu,\nu}]$. Then,

$$\phi_{\mu,\nu}^{(2)} = \frac{1}{2}\left(1 - \frac{\mu^2}{\zeta_{\mu,\nu}^2}\right). \quad (9)$$

Since $\zeta_{\mu,\nu}$ is always larger than μ, we have

$$0 < \phi_{\mu,\nu}^{(2)} \leq \frac{1}{2} \quad (10)$$

and up to first order $\phi_{\mu,\nu}^{(2)}$ is independent of μ and ν. While no closed form exists for $\phi_{\mu,\nu}^{(3)}$, it too, is found to be bounded:

$$0 < |\phi_{\mu,\nu}^{(3)}| \leq |\phi_{0,1}^{(3)}| = 0.44. \quad (11)$$

The function $\phi_{\mu,\nu}^{(4)}$ does not converge for $\nu \to \infty$, but it grows sufficiently slowly that for the first twenty

mode numbers it is contained in a relatively small interval:

$$0 < \phi_{\mu,\nu}^{(4)} \le \phi_{0,20}^{(4)} = 2.3 \qquad (\mu, \nu \le 20). \tag{12}$$

The observations (10–12) are important, because the (non)linear spring constants depend on the mode numbers μ and ν through the function $\phi_{\mu,\nu}^{(p)}$.

	$\phi_{\mu,\nu}^{(2)}$		
	$\nu = 1$	$\nu = 2$	$\nu = 3$
$\mu = 0$	1/2	1/2	1/2
$\mu = 1$	0.353	0.482	0.493
$\mu = 2$	0.286	0.456	0.480
	$\phi_{\mu,\nu}^{(3)}$		
$\mu = 0$	-0.437	0.259	-0.236
	$\phi_{\mu,\nu}^{(4)}$		
$\mu = 0$	1.28	1.48	1.61
$\mu = 1$	0.290	0.837	1.03
$\mu = 2$	0.223	0.704	0.891

Table 1: Coefficients $\phi_{\mu,\nu}^{(p)} = \frac{\int_0^{\zeta_{\mu,\nu}} J_\mu^p[q]\, q\, \mathrm{d}q}{\zeta_{\mu,\nu}^2 J_\mu^p[\zeta_{\mu,\nu}]}$ for $p = \{2, 3, 4\}$ with $\zeta_{\mu,\nu}$ the νth zero of J_μ'.

With Eq. (4), (8) and (9), we can then expose the dependence of the (non)linear spring constants on the film thickness d and confinement radius R:

$$k = (1 + \delta_{\mu 0})\, 3\pi\, \rho a_{\text{vdw}}\, \phi_{\mu,\nu}^{(2)}\, \frac{R^2}{d^4} \tag{13}$$

$$= (1 + \delta_{\mu 0})\, \frac{3\pi}{2}\, \rho a_{\text{vdw}} \left(1 - \frac{\mu^2}{\zeta_{\mu,\nu}^2}\right) \frac{R^2}{d^4}, \tag{14}$$

$$\beta = -\delta_{\mu 0}\, 12\pi\, \rho a_{\text{vdw}}\, \phi_{0,\nu}^{(3)}\, \frac{R^2}{d^5} \tag{15}$$

and

$$\alpha = (3 + 5\delta_{\mu 0})\, \frac{5\pi}{2}\, \rho a_{\text{vdw}}\, \phi_{\mu,\nu}^{(4)}\, \frac{R^2}{d^6}. \tag{16}$$

Single-phonon transition resonances from perturbation theory

The nonlinear Hamiltonian can be written, with $\lambda \ll 1$ a dimensionless parameter, as the sum $H = H_0 + \lambda H_1$ of the unperturbed Hamiltonian

$$H_0 = \frac{p^2}{2m_{\text{eff}}} + \frac{1}{2} k\, x^2 \tag{17}$$

and the perturbation

$$H_1 = \frac{1}{3}\beta x^3 + \frac{1}{4}\alpha x^4. \tag{18}$$

Then, within first order perturbation theory,

$$\begin{aligned}
\lambda E_n^{(1)} &= \langle n|\, \lambda H_1\, |n\rangle \\
&= \lambda \frac{\beta}{3} x_{\text{zpf}}^3 \langle n|\, (a + a^\dagger)^3\, |n\rangle + \lambda^2 \frac{\alpha}{4} x_{\text{zpf}}^4 \langle n|\, (a + a^\dagger)^4\, |n\rangle \\
&= 0 + \lambda \frac{3x_{\text{zpf}}^4 \alpha}{2}\left(n^2 + n + \frac{1}{2}\right) \tag{19}
\end{aligned}$$

and through second order perturbation theory,

$$\begin{aligned}
\lambda^2 E_n^{(2)} &= \sum_{k \ne n} \frac{|\langle k|\, \lambda H_1\, |n\rangle|^2}{E_n^{(0)} - E_k^{(0)}} \\
&= \frac{\lambda^2}{\hbar\Omega_\text{m}} \left(-\frac{\alpha^2}{8} x_{\text{zpf}}^8 \left(34n^3 + 51n^2 + 59n + 21\right) \right. \\
&\quad \left. - \frac{\beta^2}{9} x_{\text{zpf}}^6 \left(30n^2 + 30n + 11\right)\right). \tag{20}
\end{aligned}$$

The energy eigenvalues of the Fock states of the harmonic oscillator then become

$$\begin{aligned}
E_n &= E_n^{(0)} + \lambda E_n^{(1)} + \lambda^2 E_n^{(2)} \\
&= \hbar\Omega_\text{m}\left(n + \frac{1}{2}\right) \\
&\quad + \lambda \frac{3x_{\text{zpf}}^4 \alpha}{2}\left(n^2 + n + \frac{1}{2}\right) \\
&\quad - \lambda^2 \frac{x_{\text{zpf}}^6 \beta^2}{9\hbar\Omega_\text{m}}\left(30n^2 + 30n + 11\right) \\
&\quad - \lambda^2 \frac{x_{\text{zpf}}^8 \alpha^2}{8\hbar\Omega_\text{m}}\left(34n^3 + 51n^2 + 59n + 21\right) \tag{21}
\end{aligned}$$

with transition energies

$$\begin{aligned}
E_{n+1} - E_n &= \Omega_\text{m}\hbar + \lambda 3(n+1)x_{\text{zpf}}^4 \left(\alpha - \lambda \frac{20}{9}\frac{x_{\text{zpf}}^2 \beta^2}{\hbar\Omega_\text{m}}\right) \\
&\quad - \lambda^2 \frac{3x_{\text{zpf}}^8}{4\hbar\Omega_\text{m}}(24 + 17n(n+2))\alpha^2. \tag{22}
\end{aligned}$$

For the systems considered here, we can identify the small factors $\frac{\alpha x_{\text{zpf}}^4}{\Omega_{\text{m}\sim}} \sim \frac{\alpha x_{\text{zpf}}^3}{k}$ and $\frac{\beta x_{\text{zpf}}^3}{\Omega_{\text{m}\sim}} \sim \frac{\beta x_{\text{zpf}}}{k}$. Indeed, they are factors of increasingly high order appearing in the Taylor expansion of the Van der Waals potential in main text Eq. (6) and (8): noting that $\alpha x^3 \ll \beta x^2 \ll k\, x$, we necessarily have $\frac{\alpha x_{\text{zpf}}^4}{\Omega_{\text{m}\sim}} \ll \frac{\beta x_{\text{zpf}}^3}{\Omega_{\text{m}\sim}}$.

For example, for the mode discussed in Figure 6 in the main text and Supplementary Figure 2 and 3, $\frac{\beta x_{\text{zpf}}^3}{k x_{\text{zpf}}^2} = 5 \times 10^{-4}$ and $\frac{\alpha x_{\text{zpf}}^4}{k x_{\text{zpf}}^2} = 8 \times 10^{-7}$.

We can thus approximate

$$\begin{aligned}
\Omega[n] &= \frac{E_{n+1} - E_n}{\hbar} \\
&= \Omega_\text{m} + \frac{\lambda 3(n+1)x_{\text{zpf}}^4}{\hbar}\left(\alpha - \lambda \frac{20}{9}\frac{x_{\text{zpf}}^2 \beta^2}{\hbar\Omega_\text{m}}\right),
\end{aligned}$$

which allows us to write the cubic nonlinearity as an effective modification to the Duffing nonlinearity.

2

Spectral function calculation with Lindblad master equation

We numerically solve the spectral function of the nonlinear resonator, using the full Lindblad master equation of the open quantum system comprising the resonator and its environment.

The Hamiltonian of the nonlinear mechanical mode $H = \frac{p^2}{2m_{\text{eff}}} + \frac{1}{2}k\,x^2 + \frac{1}{3}\beta x^3 + \frac{1}{4}\alpha x^4$ can be written in terms of the eigenstates $|j\rangle$ and eigenvalues E_j as $H = \sum_j E_j \,|j\rangle\langle j|$. The eigenstates and eigenvalues are obtained by numerically discretizing and diagonalizing the Hamiltonian.

The oscillation amplitude can be written in terms of the eigenbasis as

$$x = \sum_{k>j} (x_{jk}\,|j\rangle\langle k| + \text{h.c.}) + \sum_j x_{jj}\,|j\rangle\langle j|, \quad (23)$$

with matrix elements $x_{jk} = \langle j |x| k\rangle$. The quantum master equation of the mechanical mode coupled to a bath of environmental modes can be derived using the standard perturbation theory approach in the eigenbasis [1]. Omitting the fast rotating terms in the system-bath coupling, we obtain the Lindblad master equation:

$$\frac{d\varrho}{dt} = -i\,[H, \varrho] + \mathcal{L}\varrho \qquad (24)$$

with

$$\mathcal{L} = \frac{\Gamma}{2}\sum_{k>j} |x_{jk}|^2 \Big((n_{\text{th}}\,[\delta E_{kj}] + 1)\,\mathcal{D}_{jk} \\ + n_{\text{th}}\,[\delta E_{kj}]\,\mathcal{D}_{kj} \Big), \qquad (25)$$

where ϱ is the density matrix of the mechanical mode, $n_{\text{th}}\,[\delta E_{kj}] = \left(e^{-\delta E_{kj}/k_B T} - 1\right)^{-1}$ is the thermal phonon occupation number at temperature T for the frequency difference $\delta E_{kj} = E_k - E_j$ between the states k and j, and

$$\mathcal{D}_{jk}\,\varrho = 2\,|j\rangle\langle k|\varrho|k\rangle\langle j| - |k\rangle\langle k|\varrho - \varrho|k\rangle\langle k| \quad (26)$$

is the Lindblad superoperator for the jump operation $|j\rangle\langle k|$. The difference between Eq. (24) and the standard master equation for a quantum harmonic oscillator stems from the nonlinearity in the Hamiltonian, which perturbs the equal energy level spacing.

Defining amplitude operators $\epsilon^+ = \sum_{k>j} x_{jk}\,|j\rangle\langle k|$ and $\epsilon^- = (\epsilon^+)^\dagger$, one can calculate the correlation function $G[\tau]$ of the mechanical amplitude as a function of the separation time τ:

$$G[\tau] = \left\langle \epsilon^-\,[t+\tau]\,\epsilon^+\,[t]\right\rangle_{t\to\infty}. \qquad (27)$$

Here we used the Heisenberg representation for the time-dependent operator ϵ such that $\epsilon[t] = e^{i\widetilde{H}t}\,\epsilon\,e^{-i\widetilde{H}t}$ with $\widetilde{H}$ the total Hamiltonian of the mechanical mode coupled to the bath modes.

Applying the quantum regression theorem [2], we write the correlation in Eq. (27) as a trace over the Hilbert space of the mechanical mode. In doing so, we introduce the stationary density matrix of the master equation (24) ϱ_{ss}, which is obtained by setting $\frac{d\varrho}{dt} = 0$ in Eq. (25). The correlation function then becomes:

$$G[\tau] = \text{Tr}_s\left[\epsilon^-\,e^{\mathcal{L}\tau}\left(\epsilon^+ \varrho_{ss}\right)\right]. \qquad (28)$$

These equations are implemented numerically [3] to find the solution of $G[\tau]$. The spectral function $S_{xx}[\Omega]$ can then be obtained as the Fourier transformation of $G[\tau]$:

$$S_{xx}[\Omega] = \frac{1}{2\pi}\int_{-\infty}^{\infty} e^{-i\Omega\tau}G[\tau]\,d\tau. \qquad (29)$$
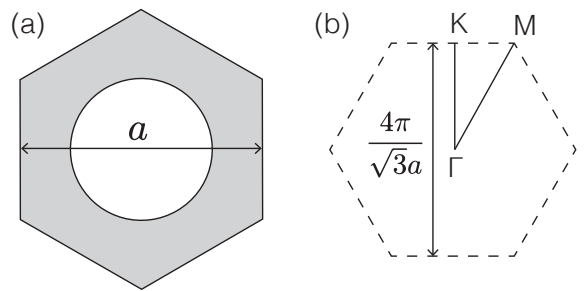
Superfluid phononic crystal

Figure 1: (a) Unit cell for hexagonal honeycomb lattice with periodicity a. (b) First Brillouin zone with symmetry points for the reduced wave vector.

We have used the finite element simulation (FEM) tool COMSOL Multiphysics® to model highly confined third sound modes in a superfluid crystal lattice by solving the hydrodynamic equations for third sound: The linearized Euler equation

$$\dot{\vec{v}} + \vec{v}\cdot\nabla\vec{v} = -\frac{3\alpha}{d^4}\vec{\nabla}\eta, \qquad (30)$$

and the continuity equation for the film height

$$\dot{\eta} + \vec{v}\cdot\vec{\nabla}\eta = -d\,\vec{\nabla}\cdot\vec{v}. \qquad (31)$$

While the software does not include ready-made solvers for the third sound, one can map the equations to those for (first) sound in an ideal gas—as outlined in Ref. [4]. From the hexagonal unit cell in Supplementary Figure 1 with lattice constant a, Floquet boundary conditions on the outer edges and free boundary conditions on the inner edge, the band structure is modeled by performing a stationary eigenfrequency analysis swept over the Floquet vector

$$\vec{k} = (k_1 b_{1x} + k_2 b_{2x}, k_1 b_{1y} + k_2 b_{2y}) \qquad (32)$$

with k_1 and k_2 dimensionless parameters between 0 and 1 to cover the entire first Brillouin zone,

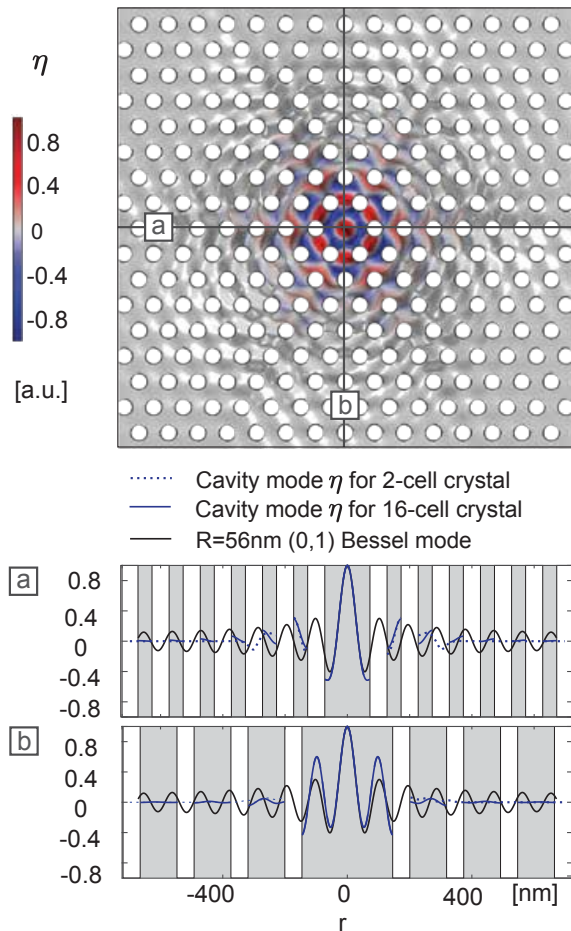$$\vec{b_1} = \left(\frac{2\pi}{a}, \frac{-2\pi}{\sqrt{3}a}\right) \qquad (33)$$

Figure 2: Mode amplitude $\eta[r, \theta]$ for 30 MHz third sound in a 11 nm thick superfluid film condensed on a suspended silicon slab (with van der Waals coefficient $a_{\text{vdw}} = 3.5 \times 10^{-24} \, \text{m}^5 \, \text{s}^{-2}$ [5]) perforated with 55 nm diameter holes and 100 nm periodicity. Panels (a) and (b) show the horizontal and vertical cross sections respectively, in comparison to the 31 MHz fundamental Bessel mode confined with free boundary conditions to a radius of 56 nm. Finite element method simulations.

the first reciprocal lattice vector, and

$$\vec{b_2} = \left(0, \frac{4\pi}{\sqrt{3}a} \right) \tag{34}$$

the second reciprocal lattice vector.

For example then, the band structure for a $d = 11$ nm thick superfluid film on an $a = 100$ nm lattice with 55 nm diameter holes is shown on Fig. 6 in the main text and is found to have a band gap between 29 and 30.5 MHz. By modeling the full crystal with a chosen amount of unit cells in either direction and the central hole removed to form a cavity, we obtained the mode amplitude $\eta[r, \theta]$ and the areal energy density

$$u = \rho\alpha \left(\frac{-\eta}{d^3} + \frac{3\eta^2}{2d^4} \right) \tag{35}$$
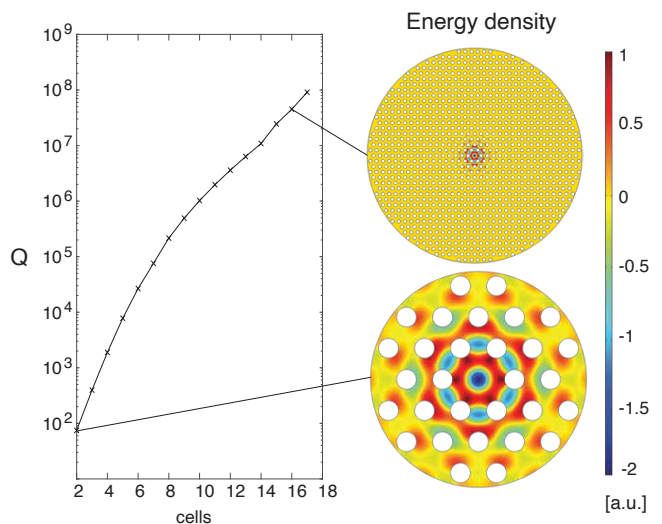

Figure 3: Finite element model of the quality factor for a 30 MHz third sound mode in 11 nm thick superfluid film condensed on a suspended silicon slab perforated with 55 nm diameter holes and crystal lattice constant 100 nm.

for the 30 MHz mode in the band gap. The amplitude η is shown in Supplementary Figure 2 for a lattice comprising approximately 16 cells in either direction. It is compared to the amplitude found for a tiny crystal comprised of only two cells in either direction. It can be seen that while the mode profiles diverge slightly farther away from the central defect, they overlap in the central region.

Since the cavity confinement in the crystal is not quite a perfectly circular confinement, it is instructive to look for the circular Bessel mode most closely resembling the profile of the trapped mode. For the present parameters, that is the $R = 56$ nm fundamental mode plotted in Supplementary Figure 2. Its frequency is 31 MHz (cf. 30 MHz for the trapped mode). From the latter, we can estimate the intrinsic single-phonon nonlinear shift: here $\delta\Omega[\alpha_{\text{eff}}]/2\pi = 35$ Hz. That means that a Q-factor $Q = \Omega_{\text{m}}/\Gamma$ in excess of 10^6, or $Q \cdot f \geq 6 \times 10^{13}$ Hz is necessary to resolve the granular nature of the resonator.

The energy density is plotted for the same two lattices on the right panel of Supplementary Figure 3. The left panel shows the quality factor associated with acoustic radiation loss. As the number of cells in the lattice increases, the quality factor increases exponentially and exceeds 10^6, the threshold for single-phonon resolution, for 10-cell lattices.

2. Supplementary Discussion

Dissipation of energy

Energy contained in superfluid ^{4}He third sound may decay through several different channels. Understanding ways energy can dissipate is especially im-

portant in the third sound resonator, since the resolution of intrinsic single-phonon statistics requires the damping Γ to be smaller than the the single-phonon resonance shift $\delta\Omega$. Experimentally, it has been observed that $Q \cdot f$ products (the product of a resonator's quality factor and frequency) in nanomechanical systems tend to lie below 10^{16} Hz [6], although much larger $Q \cdot f$ values exceeding 10^{19} have been reached recently by use of phononic crystal cavities [7]. It nonetheless is reasonable to require Qf products for single-phonon nonlinear third-sound resonators to lie below that limit, within the regime of operation of the majority of nanomechanical resonators.

Firstly, dissipation mechanisms involving the role of large densities of pinned vortices have been proposed to account for the observed dissipation in experiments [8,9]. Our recent work on optomechanical detection of vortices however appears to rule out such large remnant vortex densities on smooth microfabricated third sound resonators [10]. In addition, the sound-vortex coupling is known from theory to increase with decreasing resonator area [4], resulting in a further reduction of vortex pinning and therefore further reduction of vortex-induced dissipation. (See main article text.)

Secondly, in the two-fluid model of superfluid third sound, the superfluid component oscillates while the normal fluid component remains stationary. This leads to temperature gradients between the colder wave peaks and warmer troughs [11], and these temperature gradients can lead to thermal energy dissipation through evaporation and recondensation of helium atoms between the peaks and troughs of the wave, as well as irreversible heat flow through the substrate [11–13]—forming in essence an analog of the thermo-elastic damping encountered in mechanical resonators [14].

Finally, a fundamental loss mechanism remains the acoustic energy radiated out of the resonator due to imperfect wave reflection at the resonator boundary—corresponding for instance to the acoustic energy lost through the pedestal in the case of a superfluid-coated microdisk or microtoroid geometry [10,15,16]. This dissipation mechanisms plays the role of clamping losses in micromechanical resonators [17], and, as in the case of solid microresonators, may be suppressed through the use of a phononic bandgap structure [18,19]. In particular, the damping Γ decreases exponentially for modes trapped in phononic lattices with an increasing number of cells.

We study in detail the process of thermal dissipation and acoustic radiation in the following two Sections.

Thermal dissipation

In the usual limit, third sound waves are treated as an oscillation in the height of the superfluid compo-
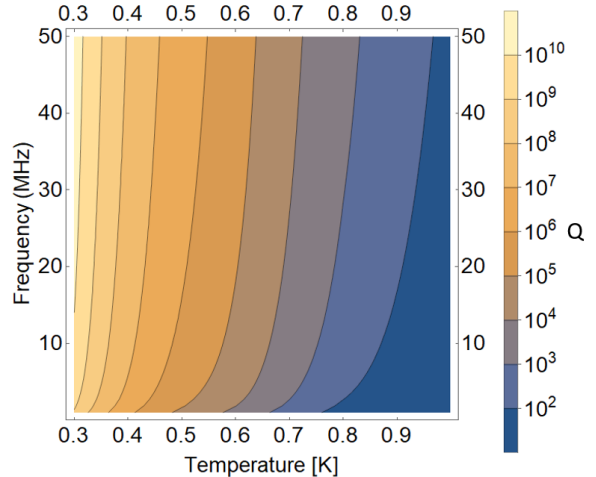

Figure 4: Third sound wave quality factor as a function of frequency and temperature for a film thickness of 11 nm. The physical properties of the film and substrate have been taken from [20–24].

nent of the film, with the normal component viscously clamped and therefore of constant height. This approximation is valid so long as the normal-fluid penetration depth $d_p = (2\mathrm{v}_n/\Omega\rho_n)^{1/2}$ is larger than the film thickness d, where v_n is the viscosity of the normal fluid and Ω is the frequency of the wave. In this case, the motion of the sound wave creates oscillating regions of high and low superfluid-to-normal fluid ratio. This changing ratio corresponds to a change in the temperature in the thin film between crests and troughs of the third sound wave. Heat will then flow from troughs to crests, dissipating energy.

Bergman derived a solution for the complex speed of third sound plane waves c_3, including both evaporation-condensation and thermal damping through the substrate [13]. However, Bergman's equations are highly complex and difficult to solve. In earlier work, Atkins presented an alternative simpler solution [11], making a series of approximations about the film thickness, thermal dissipation mechanisms and third sound frequency. In the thick film/high frequency limit (as would be the case here), attenuation of third sound is dominated by the phenomenon of evaporation and condensation of helium atoms between the film and the gas [13]. In this limit, the attenuation derived by Atkins differs from Bergman's more complete analysis only by a factor of $16/9$ [13], and provides therefore a reasonable estimate of the expected magnitude of the thermal damping. Atkins' expression for the complex third sound speed c_3 is given by [11]:

$$c_3^2 = \frac{\frac{\rho f d}{\rho_{\mathrm{He}}} + \frac{\rho S T}{\rho_{\mathrm{He}}}\left[\left(S - \frac{\beta}{\rho_{\mathrm{He}}}\right) - i\frac{Kf}{\rho_{\mathrm{He}}\Omega}\right]}{C - i\frac{KL}{\rho_{\mathrm{He}}\Omega d}} \quad (36)$$

Where ρ_{He} and ρ are the total fluid density and super-

fluid component density, respectively, d is the depth of the film and f is the van der Waals force per unit mass at the surface of the film [20]. C, S and L are the specific heat, entropy and latent heat of evaporation of the film [21]. β is the slope of the vapour pressure curve and K is the mass flow from evaporation both taken from the Vapour Pressure data published by Donnelly and Barenghi [21]. Solving this equation for c_3 gives the quality factor Q of the third sound wave via $Q = \Re(c_3)/2\Im(c_3)$.

We use Eq. (36) here to determine the thermal dissipation dominated quality factor for a third sound wave on a silica substrate as a function of temperatures, film thicknesses and third sound frequencies.

Supplementary Figure 4 shows the thermal dissipation dominated Q for an 11 nm thick film as a function of temperature and oscillation frequency. We chose a frequency range of 1 to 50 MHz , consistent with the range of third sound mechanical resonance frequencies expected for confinement length scales ranging from tens of nanometres to a micron with this film thickness. We choose a temperature range of 0.3 to 1.0 K, easily achievable using a standard dilution refrigerator or helium-3 cryostat. From the figure we can see that the quality factor improves dramatically with decreasing temperature, and that it increases with increasing frequency. This rise with frequency is expected from Eq. (36), where high frequencies suppresses the complex component responsible for the damping. This effect of high frequency reducing damping also arises in thermoelastic damping where there is a characteristic time for the temperature fluctuation from a deflected beam to diffuse. At high frequency the system does not have sufficient time to respond to the change in temperature, reducing the diffusion of heat through the system and increasing the Q [25]. The thermal-dissipation-dominated quality factor exceeds 10^6 for the entire frequency range for temperatures beneath 0.4 K.
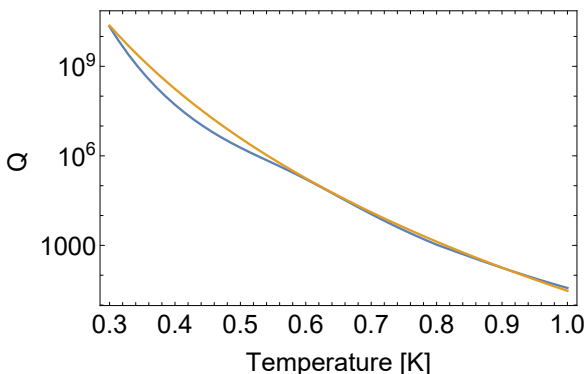

Figure 5: Third sound wave quality factor as a function of temperature at 30 MHz for a 11 nm thick film. The yellow line: rough fit to a T^{17} dependence.

At low temperature the film has almost no normal fluid component. The difference in the proportion

of superfluid component at the peaks and troughs of the third sound wave is reduced as a result, which reduces the temperature gradient. This causes the thermal damping to drop significantly as the normal fluid fraction drops. This dependence can be seen in Supplementary Figure 5. The third sound wave frequency and film thickness in this case are chosen to match the phononic crystal cavity mode shown in Fig. 6(b) of the main text. As can be seen, the predicted thermal-dissipation-dominated quality factor exceeds 10^6 at temperatures beneath 0.5 K, so that (as discussed in the main text) thermal dissipation should not preclude reaching the single phonon nonlinear regime. The fit in Supplementary Figure 5 shows a rough temperature dependence of $Q \propto T^{17}$, showing the dramatic suppression of thermal dissipation with decreasing temperature.
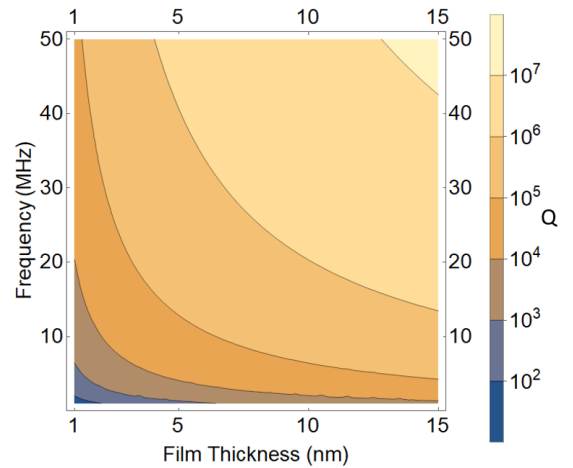

Figure 6: Third sound quality factor as a function of film thickness and frequency, at a temperature of 400 mK.

Supplementary Figure 6 shows the dependence of the thermal-dissipation-dominated third sound quality factor on frequency and film thickness for a fixed temperature of 0.4 K. This shows that the quality factor is predicted to decrease as the film thickness reduces. It also illustrates, again, the strong increase in quality factor predicted with increasing frequency.

Critical velocity

Liquid helium retains its superfluidity only as long as the particle velocity in the fluid v remains below its critical velocity v_c, i.e. $\frac{v}{v_c} < 1$. Since this work is concerned with strong confinement of superfluid films, it is important to verify that superfluidity is retained for all radii R and film thicknesses d considered. From Ref. [11], $v/v_c = \frac{\rho}{\rho_{\mathrm{He}}} \frac{<x>}{d}$ [11].
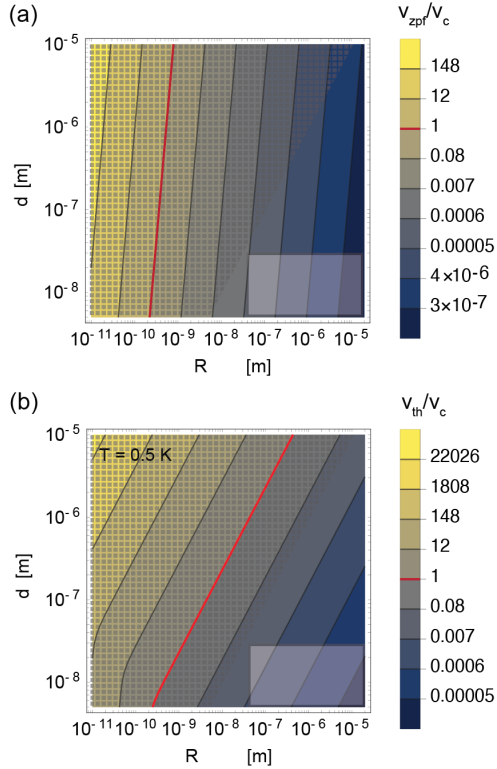
Figure 7: Ratio of superfluid particle velocity to critical velocity v_c. (a) Zero-point motion velocity v_{zpf} and (b) thermal motion velocity v_{th} at $0.5\,K$. Shaded: regime of single-phonon nonlinear third-sound resonator. Red lines indicate $v_{zpf} = v_c$ and $v_{th} = v_c$ crossovers. Hatched: region outside of validity of this work ($d \geq R$)

We consider two cases, first the case where the third sound mode is cooled to its motional ground state, and second the case where it is thermalized at temperature T. In the former case, the velocity ratio is

$$\frac{v_{zpf}}{v_c} = \frac{\rho}{\rho_{He}} \frac{x_{zpf}[R,d]}{d}, \qquad (37)$$

where v_{zpf} is the zero point velocity, while in the latter case it is

$$\frac{v_{th}}{v_c} = \frac{\rho}{\rho_{He}} \frac{x_{zpf}[R,d]}{d} \sqrt{1 + \frac{2}{e^{\sim \Omega_m[R,d]/k_B T} - 1}}. \quad (38)$$

In Supplementary Figure 7 we show these two ratios as a function of the radius of the third sound mode and the superfluid film thickness, taking $T = 0.5\,K$ for the thermalized mode. It can be seen from these figures that the regime of operation we consider in the main text for nonlinear superfluid resonators (shaded) lies far outside of the regime where superfluidity breaks down, both for a third-sound resonator in its ground state (Supplementary Figure 7a) and for one cooled to $0.5\,K$ (Supplementary Figure 7b). Even in the most extreme parameters probing the limits of our model ($T = 0.5\,K$, $R = 20$ nm, $d = 5$ nm),

the particle velocity remains two orders of magnitude lower than the critical velocity ($v_c = 250\,v_{th}$).

We finally note that, while it might be expected that the particle velocity would increase with decreasing film thickness from the explicit inverse-d dependence of both Eqs. (37) and (38), in fact the opposite is predicted. This is due to the dependence of the resonator's spring constants and zero-point motion on the film thickness d, as derived in Eq. (9-11) and (23) in the main text.

Supplementary References

[1] Gardiner, C. & Zoller, P. *Quantum Noise*. Springer Series in Synergetics (Springer, 2004), 3 edn.

[2] Lax, M. Formal theory of quantum fluctuations from a driven state. *Phys. Rev.* **129**, 2342–2348 (1963).

[3] Tan, S. M. A computational toolbox for quantum and atomic optics. *J. Opt.* **1**, 424–432 (1999).

[4] Forstner, S. *et al.* Modelling of vorticity, sound and their interaction in two-dimensional superfluids. *New J. Phys.* **21**, 053029 (2019).

[5] Sabisky, E. S. & Anderson, C. H. Onset for superfluid flow in he^4 films on a variety of substrates. *Phys. Rev. Lett.* **30**, 1122–1125 (1973).

[6] Aspelmeyer, M., Kippenberg, T. J. & Marquardt, F. Cavity optomechanics. *Rev. Mod. Phys.* **86**, 1391–1452 (2014).

[7] Ren, H. *et al.* Two-dimensional optomechanical crystal cavity with high quantum cooperativity. *Nat. Commun.* **11**, 3373 (2020).

[8] Penanen, K. & Packard, R. E. A Model for Third Sound Attenuation in Thick 4He Films. *J. Low Temp. Phys.* **128**, 25–35 (2002).

[9] Hoffmann, J. A., Penanen, K., Davis, J. C. & Packard, R. E. Measurements of attenuation of third sound: Evidence of trapped vorticity in thick films of superfluid 4he. *J. Low Temp. Phys.* **135**, 177–202 (2004).

[10] Sachkou, Y. P. *et al.* Coherent vortex dynamics in a strongly interacting superfluid on a silicon chip. *Science* **366**, 1480–1485 (2019).

[11] Atkins, K. R. Third and fourth sound in liquid helium II. *Phys. Rev.* **113**, 962–965 (1959). arXiv:1011.1669v3.

[12] Bergman, D. Hydrodynamics and Third Sound in Thin He II Films. *Phys. Rev.* **188**, 370–384 (1969).

[13] Bergman, D. J. Third sound in superfluid helium films of arbitrary thickness. *Phys. Rev. A* **3**, 2058–2066 (1971). arXiv: 1011.1669v3.

[14] Lifshitz, R. & Roukes, M. L. Thermoelastic damping in micro- and nanomechanical systems. *Phys. Rev. B* **61**, 5600–5609 (2000).

[15] Harris, G. I. *et al.* Laser cooling and control of excitations in superfluid helium. *Nat. Phys.* **12**, 788–793 (2016).

[16] He, X. *et al.* Strong optical coupling through superfluid brillouin lasing. *Nat. Phys.* (2020).

[17] Nguyen, D. T. *et al.* Ultrahigh Q-frequency product for optomechanical disk resonators with a mechanical shield. *Appl. Phys. Lett* **103**, 241112 (2013).

[18] Tsaturyan, Y., Barg, A., Polzik, E. S. & Schliesser, A. Ultracoherent nanomechanical resonators via soft clamping and dissipation dilution. *Nat. Nanotechnol.* **12**, nnano.2017.101 (2017).

[19] Condat, C. A. & Kirkpatrick, T. R. Third-sound propagation on a periodic substrate. *Phys. Rev. B* **32**, 4392 (1985).

[20] Baker, C. G. *et al.* Theoretical framework for thin film superfluid optomechanics: Towards the quantum regime. *New J. Phys.* **18**, 123025 (2016). 1609.07265.

[21] Donnelly, R. J. & Barenghi, C. F. The Observed Properties of Liquid Helium at the Saturated Vapor Pressure. *J. Phys. Chem. Ref. Data* **27**, 1217–1274 (1998). Publisher: American Institute of Physics.

[22] Jensen, J., Stewart, R. G., Tuttle, W. & Brechna, H. *Brookhaven national laboratory selected cryogenic data notebook: sections I-IX*, vol. 1 (Brookhaven National Laboratory, 1980).

[23] Molinari, V., Mostacci, D. & Ganapol, B. D. The specific heat of liquid helium. *J. Comput. Theor. Transp.* **45**, 212–218 (2016).

[24] Zeller, R. & Pohl, R. Thermal conductivity and specific heat of noncrystalline solids. *Phys. Rev. B* **4**, 2029 (1971).

[25] Schmid, S., Villanueva, L. G. & Roukes, M. L. *Fundamentals of nanomechanical resonators*, vol. 49 (Springer, 2016).